One-Way Valley-Robust Transport in Edge-Tailored Photonic Crystals

Jianfeng Chen,[1,*] Yidong Zheng,[2,*] Shuihua Yang,[1] Fulong Shi,[1] Zhi-Yuan Li,[2,†] and Cheng-Wei Qiu[1,‡]
[1]Department of Electrical and Computer Engineering, National University of Singapore, Singapore 117583, Singapore
[2]School of Physics and Optoelectronics, South China University of Technology, Guangzhou 510640, China

(Received 13 January 2025; revised 24 March 2025; accepted 1 May 2025; published 22 May 2025)

Valley photonics, with its rapid advancements and immense potential, lays one pivotal cornerstone toward next-generation topological photonic devices. It enables valley-polarized topological states, whose valleys are intrinsically locked up with transmission directivity. However, these states are prone to defects in photonic structures, and backscattering may easily induce valley flipping. Hence, achieving a one-way valley-robust photonic crystal, immune to perturbations, remains elusive. Here, we demonstrate a one-way, valley-polarized state in an edge-tailored photonic crystal that is robust against defects. Such crystal possesses a Chern band gap and is achieved without using an interface between two crystals with opposite Berry curvatures. We show K-valley-robust transport in a defective crystal and demonstrate perfect conversion between the K and K' valleys in a hybridized crystal while backscattering is greatly suppressed. Our results offer a promising approach for unidirectional control of the valley degrees of freedom in light.

DOI: 10.1103/PhysRevLett.134.203803

Introduction—One-way transport of information carriers is essential for contemporary information and communication technology [1–3]. Recently, the valley, as a pseudospin degree of freedom, has been employed to achieve valley-selective unidirectional transport in electronic materials [4,5]. Inspired by these developments, valley photonic crystal has been proposed [6,7]. It supports photonic valley-polarized topological states whose transport directions are locked with the valleys. Similar effects have also been extensively investigated in phononic systems [8–11]. These states power up numerous applications for valley-based information encoding and processing [12–21].

Breaking parity-inversion symmetry results in valley photonic crystals, where two valleys feature opposite local Berry curvatures [6–21]. By creating a line defect between crystals with opposite Berry curvatures, valley states can be realized [22–24], see Figs. S1 and S2 in Supplemental Material for more details [25]. However, nonglobal topology of valley photonic crystals determines that imperfections will lead to backscattering, consequently causing valley flipping [28–30]. An advancement has been made in reducing backscattering in valley phononic crystals [31] via dissipative dilution. Since it still relies on strict crystal symmetry, this phononic approach still encounters the inevitable intrinsic backscattering, frequency-specific operation, and defect brittleness (Fig. S3) [25]. Therefore, the question remains whether one-way valley-robust states that are immune to defects can be realized.

A Chern photonic crystal with a one-way topological state can be created by breaking time-reversal symmetry [32–36]. These states are protected by a nonzero Chern number, determined by globally integrating the Berry curvature over the entire Brillouin zone. However, unlike the valley state, this state is independent of the valleys. A natural idea is to combine the two, creating a one-way valley-polarized topological state, which could potentially lead to a Chern-protected and valley-robust state. However, it is generally understood that a valley photonic crystal requires breaking parity-inversion symmetry, while a Chern photonic crystal requires breaking time-reversal symmetry. As a result, the bulk-tailored global competition between these two symmetries [Fig. 1(a)] typically leads to a "one or the other" scenario—namely, the band gap supports either a valley state or a one-way state [37–42], rather than a one-way valley-polarized state.

Here, we theoretically and experimentally realize a one-way, valley-robust state in a gyromagnetic photonic crystal through engineering both bulk magnetic bias and edge geometry. The key is to introduce the valley degree of freedom of one-way state through local configuration of edge geometry, rather than relying on the global breaking of parity-inversion symmetry [Fig. 1(a)]. Specifically, the bulk magnetic bias breaks the time-reversal symmetry of the systems, opening a Chern band gap that hosts a one-way valley-independent state. Meanwhile, the edge-tailored geometry introduces the valley degree of freedom into the one-way states without disturbing the bulk topology [43–47]. As a result, Chern-protected, valley-robust one-way edge states emerge, with the valley degree of freedom remaining continuously tunable. This strategy avoids the global competition between the parity-inversion symmetry

*These authors contributed equally to this work.
†Contact author: phzyli@scut.edu.cn
‡Contact author: chengwei.qiu@nus.edu.sg

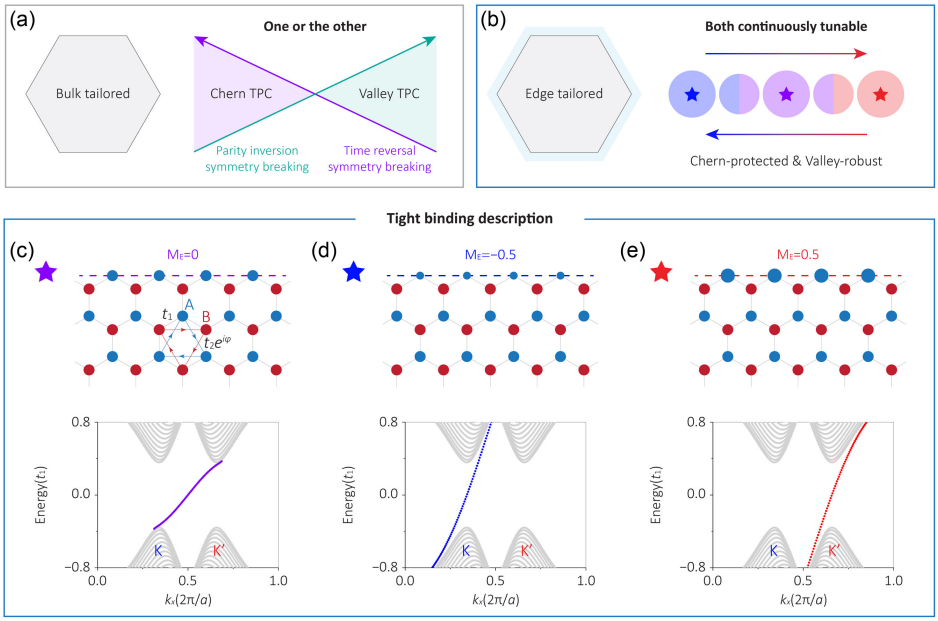

FIG. 1. One-way valley-robust topological states. (a) Topological phase transitions driven by a bulk-tailored global competition between parity-inversion symmetry (cyan) and time-reversal symmetry (purple). (b) A Chern-protected, valley-robust state can be created in an edge-tailored photonic crystal. Tailoring edge configuration (light blue area) drives the one-way state from valley independent (purple) to valley polarized (blue and red). (c)–(e) Tight-binding model. Sublattices A and B are denoted by blue and red circles, respectively. (c) One-way valley-independent topological state at $M_E = 0$. (d) One-way K-valley-polarized topological state at $M_E = -0.5$. (e) One-way K'-valley-polarized topological state at $M_E = 0.5$.

and the time-reversal symmetry, and breaks the intuition that two valley photonic crystals with opposite Berry curvatures are typically necessary to realize valley states [6,7].

Tight-binding description—We establish an effective tight-binding description by tailoring global next-nearest-neighbor coupling and local on-site potential on the edge [Figs. 1(c)–1(e)]. The semi-infinite honeycomb lattice of a lattice constant $a = 1$ with zigzag edge. The Hamiltonian is described by $H = t_1 \sum_{\langle i,j \rangle} c_i^\dagger c_j + t_2 \sum_{\langle\langle i,j \rangle\rangle} e^{-iv_{ij}\varphi} c_i^\dagger c_j + M \sum_i \varepsilon_i c_i^\dagger c_i + M_E \sum_E \varepsilon_E c_E^\dagger c_E$, where c_i is the annihilation operator at an A sublattice site in the nth unit cell, with an analogous definition for c_j. $v_{ij} = \pm 1$ accounts for the alternating sign of the magnetic phase of second-neighbor coupling and $\varphi = \pi/2$. $\varepsilon_i = +1(-1)$ when i refers to the $A(B)$ sublattice sites. The global parameters $t_1 = 1$, $t_2 = 0.05$, and $M = 0$ are the strengths of the nearest-neighbor coupling, the second-neighbor coupling, and the parity-inversion-breaking on-site potential, respectively, while the local parameter M_E represents the on-site potential on the edge.

When $M_E = 0$, an edge band (purple) appears within a Chern band gap, connecting the K and K' valleys [Fig. 1(c)]. Since the edge band spans both valleys, the resulting topological transport is valley independent. As M_E decreases to -0.5 (blue), the edge band bends upward and becomes localized around the K valley [Fig. 1(d)]. Importantly, the bulk band remains unchanged during this process, indicating that the local tailored edge potential does not destroy the global bulk topology. As a result, a one-way K-valley-polarized topological state emerges. Conversely, when M_E increases to 0.5 (red), the edge band bends downward and localizes around the K' valley [Fig. 1(e)], giving rise to a one-way K'-valley-polarized topological state. These results demonstrate that one-way valley-polarized topological state can be realized within a Chern band gap by tailoring the edge potential. This unveils the underlying mechanism behind valley-robust unidirectional transport and provides a general approach for controlling valley degrees of freedom in waves.

Photonic designs—Let us further consider a two-dimensional gyromagnetic photonic crystal composed of gyromagnetic cylinders (yttrium iron garnet, YIG), arranged in a honeycomb lattice [Fig. 2(a)]. Gyromagnetic photonic crystals have long served as an essential system for exploring various topological phenomena [48]. The material properties can be seen in Supplemental Material [25]. Figure 2(b) shows the Brillouin zone and high-symmetry points. An external magnetic field of $B = 0.12$ T is applied along the axis of gyromagnetic cylinders (i.e., $+z$ *direction*), and the time-reversal symmetry of the system is broken. As a result, a Chern band gap emerges [Fig. 2(c)]. The Chern number of the first band is -1 (Fig. S4) [25]. The phase distribution of the E_z field reveals that the bulk modes at the K and K' points exhibit phase vortices [Fig. 2(d)]. Because of the breaking of time-reversal symmetry, both vortices decrease by 2π in the counterclockwise direction (as indicated by magenta

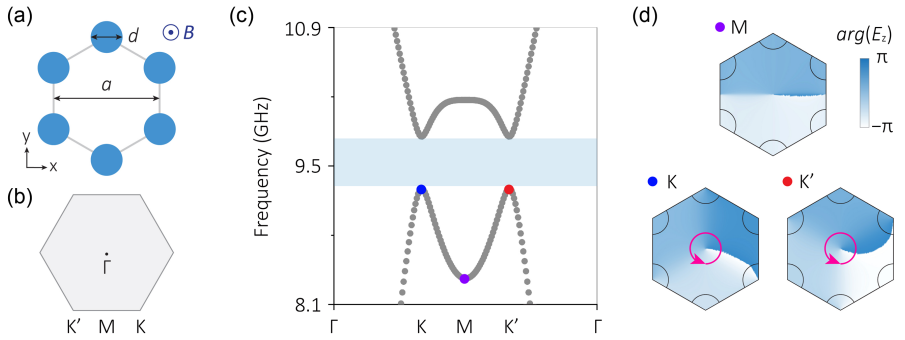

FIG. 2. Photonic crystal and its bulk dispersions. (a) Schematic of unit cell of a honeycomb lattice under an external magnetic field (B). The lattice constant is $a = 1.0$ cm, and the diameter of the cylinders is $d = 0.3a$. The external magnetic field is applied along the $+z$ direction. (b) Brillouin zone and high-symmetry points. (c) Two lowest bulk bands of gyromagnetic photonic crystal. A Chern band gap (blue area) is found between the first and second bulk bands (gray points). (d) Phase distributions of the E_z field for the first band bulk modes at the K (blue), M (purple), and K' (red) points.

arrows), resulting in an orbital angular momentum with a topological charge $l = \oint_L \nabla[\arg(E_z)]d\vec{s}/2\pi = 1$, where L is a closed contour surrounding the unit cell center [49]. The E_z field with orbital angular momentum of $l = 1$ corresponds to an in-plane magnetic field $\vec{H}_{\parallel}$ with right-handed spin angular momentum at the origin. Consequently, the valley-polarized states can be excited by external sources with right-handed chirality. In contrast, the E_z field at the M point remains independent of the valleys. Thus, it lacks phase vortices and can be excited by sources with any chirality [Fig. 2(d)].

Photonic identifications—Figures 3(a)–3(c) illustrate an edge constructed by a semi-infinite gyromagnetic photonic crystal at the bottom and a metallic cladding at the top. The experimental samples and measurements can be seen in Figs. 3(m)–3(o) and S5 [25]. The projected band structure is calculated by adopting a supercell in one column along the y direction. In experiment, the edge band is measured by applying one-dimensional Fourier transform to the complex electric field at the edge [50], see Supplemental Material for more details [25]. For the original photonic crystal, the diameters of the cylinders on the bulk and the outmost edge (purple dotted line) are the same (i.e., $d = d_E = 0.3a$). A one-way state emerges in a Chern band gap ranging from 9.2 to 9.8 GHz. The measured dispersion is consistent with the simulation result [Fig. 3(d)]. The edge band is distributed between K and K' valleys, indicating that one-way state is independent of the valleys. We design a chirality source to generate clockwise or anticlockwise phase vortex, to construct LCP or RCP sources [Figs. 3(m)–3(o) and S6] [25]. It thus enables us to selectively excite the valley-polarized states that depend on different valleys. We directly observe the explicit transport behaviors in real space by using direct near-field mapping. One can see that both LCP and RCP light can excite the right-propagating one-way state [$k_x = 1/2(2\pi/a)$, Figs. 3(g) and 3(j)], expected from the edge dispersions.

As d_E decreases from $0.3a$ to $0.2a$ [Fig. 3(b)], the edge band bends upward [Figs. S7(d)–S7(h)] and eventually connects the upper and lower bands around the K valley [Fig. 3(e)], see Supplemental Materials for more details [25]. This change neither disrupts the bulk topology nor mixes different valleys, but it drives a transition of the one-way state from being valley independent to valley polarized. When both LCP and RCP sources excite the edge state, LCP light fails to induce any guided states [Fig. 3(k)], while RCP light can excite the right-propagating one-way K-valley state [$k_x = 1/3\ (2\pi/a)$, Fig. 3(h)]. Similarly, as d_E varies from $0.3a$ to $0.4a$ [Fig. 3(c)], the edge band bends downward [Figs. S7(h)–S7(l)] and eventually distributes around the K' valley [Fig. 3], see Supplemental Material for more details [25]. For $d_E = 0.4a$, only RCP light can excite the one-way K'-valley state [$k_x = 2/3\ (2\pi/a)$], transporting rightwards [Fig. 3(i)], while LCP light fails to induce any guided states [Fig. 3(l)]. These results are consistent with the bulk modes at the K and K' valleys, which exhibit right-circular orbital angular momentum. Additionally, the evolution of edge bands varying with d_E from $0.08a$ to $0.52a$ can be seen in Fig. S7 [25]. The experimental samples and simulation results are shown in Figs. S8 and S9 [25]. We also show that these one-way valley-robust states can continuously bypass sharp corners and obstacles, while maintaining their valley in a reflectionless way (Fig. S10) [25]. Although geometric imperfections and measurement limitations introduce slight differences between the experimental and simulated results, both clearly demonstrate one-way valley-robust transport. Further details can be found in Supplemental Material [25]. In addition, we provide simulations of the edge state transport in photonic crystal with position perturbations, revealing the strong robustness of our design to realistic fabrication imperfections (Figs. S11 and S12) [25].

Photonic applications—Beyond the one-way valley-robust transport, the above results also imply that the topological channels can overcome longstanding challenges, such as backscattering loss, limited operation bandwidth, and impedance mismatching in conventional

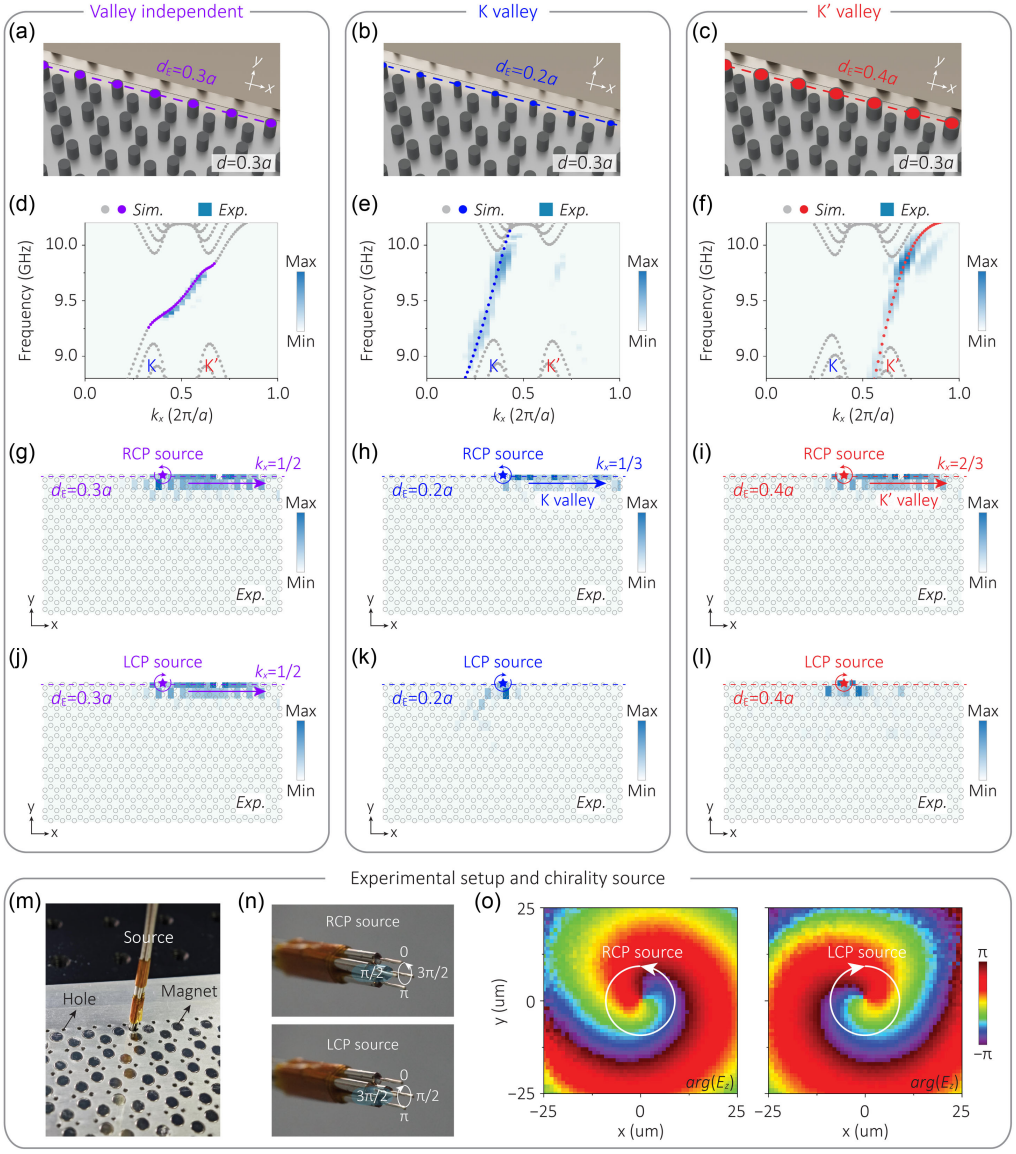

FIG. 3. Observation of one-way valley-robust states. (a)–(c) A close view of the sample bounded with a metallic cladding. The diameter of the cylinders inside the bulk is $d = 0.3a$. The diameters of the outmost cylinders are (a) $d_E = 0.3a$ (purple), (b) $d_E = 0.2a$ (blue), and (c) $d_E = 0.4a$ (red), respectively. The distance from the metallic boundary to the center of the first row of YIG rods is $0.44a$. (d)–(f) Calculated and measured dispersions. The color points and maps denote the simulated values and measured data, respectively. (g)–(l) Experimental mappings of topological states excited by (g)–(i) RCP and (j)–(l) LCP sources at a frequency of 9.5 GHz. (a),(d),(g),(j) One-way valley-independent state at $d_E = 0.3a$. (b),(e),(h),(k) One-way K-valley-polarized state at $d_E = 0.2a$. (c),(f),(i),(l) One-way K'-valley state at $d_E = 0.4a$. (m) Close-up top view of the experimental sample and measurement. The antenna is inserted into the sample holes to measure the signal point by point. (n) Chirality source composed of a four-antenna array connected to four phase shifters. (o) Measured phase distribution of E_z field around the chirality sources.

valley-based devices. As prototypical examples, we experimentally demonstrate the valley-robust channels that are immune to the backscattering and impedance mismatching, see Figs. 4(a)–4(b) and S13 in Supplemental Material [25]. Specifically, when twelve gyromagnetic cylinders of the edge are replaced by metallic cylinders (yellow), a defective crystal is created. The K-valley state unidirectionally transports forward around the scatterers without valley flipping [Fig. 4(c)]. These measured results are consistent with the simulation results in Fig. S14(a) [25]. Figure 4(e) displays the simulated Fourier spectra, with intensity indicated by a color map, on both sides of the obstacle. This is obtained through a Fourier transformation of the simulated field distribution shown in Fig. S14(a) [25]. This clearly demonstrates that only K valleys are excited, despite the introduction of obstacle on the transport path. The parameters of S_{21} and S_{12} represent the transmission coefficients of rightward and leftward propagation, respectively.

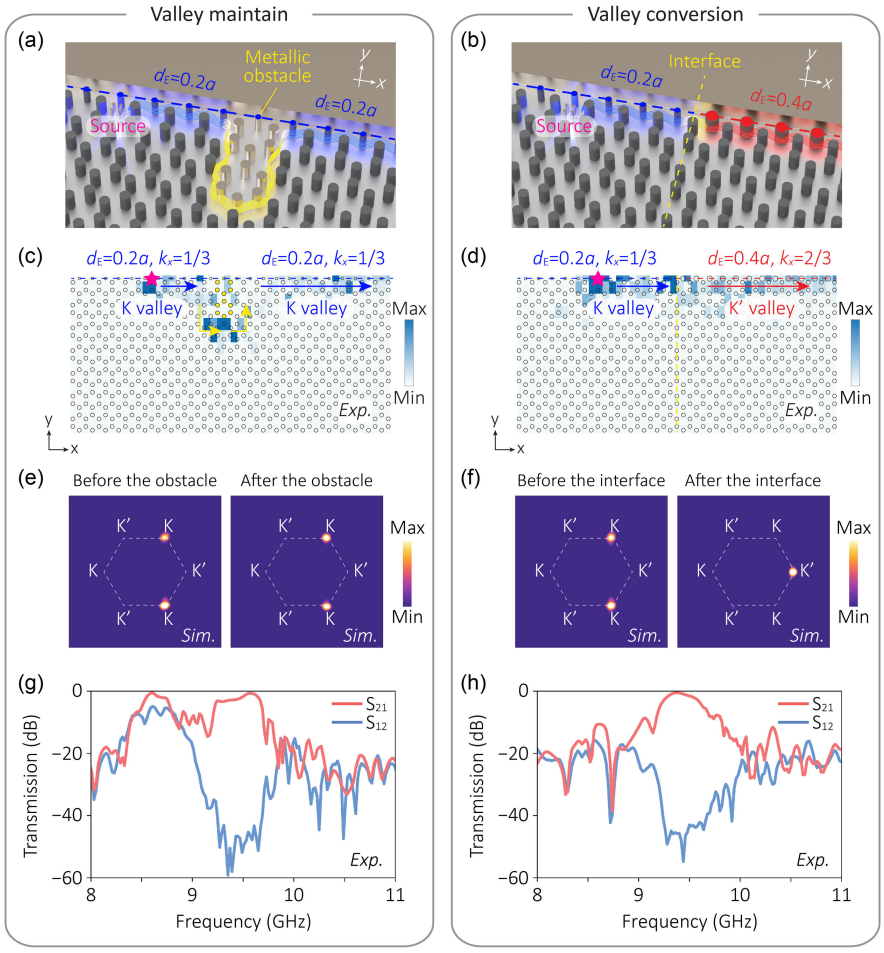

FIG. 4. Photonic applications of one-way valley-robust states. (a),(b) Top view of the sample. (c),(d) Measured electric field distributions. (e),(f) Simulated Fourier spectra at a frequency of 9.5 GHz, indicated by a color map, obtained by a Fourier transformation of the simulated field distribution shown in Fig. S14 [25]. (g),(h) Measured transmission spectra for valley-robust crystal. (a),(c),(e),(g) Valley maintain in a defective crystal. K-valley state unidirectionally bypasses the metallic obstacle without valley flipping. (b),(d),(f),(h) Valley conversion in a hybridized crystal. K-valley state perfectly converts to K'-valley state without requiring impedance matching.

The transmission spectrum illustrates that this K-valley channel maintains a very high nonreciprocity across a wide bandwidth (about 45 dB at 9.2–9.8 GHz).

We proceed to construct a hybrid crystal comprising two distinct regions ($d_E = 0.2a$ and $0.4a$), each supporting one-way K- and K' valley states, respectively [Fig. 4(b)]. The interface between these regions is depicted by a yellow dotted line. This heterostructure collectively forms a topological system with a nonzero Chern number. Consequently, the hybrid crystal is immune to the impedance mismatching, as scattering is strictly forward. This ensures the perfect conversion of one-way state from K valley to K' valley. Figures 4(d) and 4(f) clearly show that the K-valley state unidirectionally transports, further converts its valley, and continues to transport rightwards in a reflection-free way, despite the serious impedance and momentum mismatching at the interface. These measurements are consistent with the simulated results in Fig. S14(b) [25]. The measured transmission spectrum also illustrates a high contrast of the hybrid crystal (approximately 45 dB from 9.2 to 9.8 GHz).

Conclusion and outlook—In summary, we have experimentally achieved a one-way valley-robust state via manipulating global bulk magnetic bias and local edge geometry of a gyromagnetic photonic crystal. By simply varying the diameters of cylinders on the outmost edge, we observe a transition of the one-way states from being valley-independent to valley-polarized, verified by dispersion calculations and measurements. We further demonstrate that the strictly forward scattering forces the topological channels to behave as backscattering-free valley-based devices operating across a wide bandwidth. Furthermore, we develop an effective tight-binding approximation by configuring global next-nearest-neighbor coupling and on-site potential on the edge to understand the appearance of the one-way valley-robust state. Although we employ YIG crystals, other materials with gyromagnetic or gyroelectric responses can also be utilized [51–53].

Lastly, extending these phenomena from two dimensions to three dimensions will provides more opportunities for topological photonics and its related applications [54]. Our findings offer a general approach for controlling valley degrees of freedom in waves. Similar effects and phenomena can also be demonstrated in other physical systems [55–60].

Acknowledgments—C.-W. Q. acknowledges financial support from the NRF, Prime Minister's Office, Singapore under the Competitive Research Program Award (NRF-CRP22-2019-0006). C.-W. Q. acknowledges support from the Ministry of Education in Singapore (Grant No. A-8002152-00-00 and No. A-8002458-00-00). Z.-Y. L. acknowledges financial support from the Science and Technology Project of Guangdong (2020B010190001) and the National Natural Science Foundation of China (12434016).

Data availability—The data that support the findings of this article are openly available [61].

[1] R. Fleury, D. L. Sounas, C. F. Sieck, M. R. Haberman, and A. Alù, Sound isolation and giant linear nonreciprocity in a compact acoustic circulator, Science **343**, 516 (2014).
[2] J. Veenstra, O. Gamayun, X. Guo, A. Sarvi, C. V. Meinersen, and C. Coulais, Non-reciprocal topological solitons in active metamaterials, Nature (London) **627**, 528 (2024).
[3] M. Scheucher, A. Hilico, E. Will, J. Volz, and A. Rauschenbeutel, Quantum optical circulator controlled by a single chirally coupled atom, Science **354**, 1577 (2016).
[4] D. Xiao, G. B. Liu, W. Feng, X. Xu, and W. Yao, Coupled spin and valley physics in monolayers of MoS_2 and other group-VI dichalcogenides, Phys. Rev. Lett. **108**, 196802 (2012).
[5] L. Ju *et al.*, Topological valley transport at bilayer graphene domain walls, Nature (London) **520**, 650 (2015).
[6] T. Ma and G. Shvets, All-Si valley-Hall photonic topological insulator, New J. Phys. **18**, 025012 (2016).
[7] J. W. Dong, X. D. Chen, H. Zhu, Y. Wang, and X. Zhang, Valley photonic crystals for control of spin and topology, Nat. Mater. **16**, 298 (2017).
[8] J. Lu, C. Qiu, L. Ye, X. Fan, M. Ke, F. Zhang, and Z. Liu, Observation of topological valley transport of sound in sonic crystals, Nat. Phys. **13**, 369 (2017).
[9] Z. Tian, C. Shen, J. Li, E. Reit, H. Bachman, J. E. S. Socolar, S. A. Cummer, and T. Jun Huang, Dispersion tuning and route reconfiguration of acoustic waves in valley topological phononic crystals, Nat. Commun. **11**, 762 (2020).
[10] M. Yan, J. Lu, F. Li, W. Deng, X. Huang, J. Ma, and Z. Liu, On-chip valley topological materials for elastic wave manipulation, Nat. Mater. **17**, 993 (2018).
[11] S. Zhao *et al.*, Topological acoustofluidics, Nat. Mater. (2025).
[12] Y. Zeng *et al.*, Electrically pumped topological laser with valley edge modes, Nature (London) **578**, 246 (2020).
[13] Y. Yang, Y. Yamagami, X. Yu, P. Pitchappa, J. Webber, B. Zhang, M. Fujita, T. Nagatsuma, and R. Singh, Terahertz topological photonics for on-chip communication, Nat. Photonics **14**, 446 (2020).
[14] F. Gao, H. Xue, Z. Yang, K. Lai, Y. Yu, X. Lin, Y. Chong, G. Shvets, and B. Zhang, Topologically protected refraction of robust kink states in valley photonic crystals, Nat. Phys. **14**, 140 (2018).
[15] X.-T. He, E.-T. Liang, J.-J. Yuan, H.-Y. Qiu, X.-D. Chen, F.-L. Zhao, and J.-W. Dong, A silicon-on-insulator slab for topological valley transport, Nat. Commun. **10**, 872 (2019).
[16] Y. Chen, X. T. He, Y. J. Cheng, H. Y. Qiu, L. T. Feng, M. Zhang, D. X. Dai, G. C. Guo, J. W. Dong, and X. F. Ren, Topologically protected valley-dependent quantum photonic circuits, Phys. Rev. Lett. **126**, 230503 (2021).
[17] Y. Chen, J. Feng, Y. Huang, W. Chen, R. Su, S. Ghosh, Y. Hou, Q. Xiong, and C.-W. Qiu, Compact spin-valley-locked perovskite emission, Nat. Mater. **22**, 1065 (2023).
[18] K. Rong *et al.*, Spin-valley Rashba monolayer laser, Nat. Mater. **22**, 1085 (2023).
[19] X. Duan, B. Wang, K. Rong, C. Liu, V. Gorovoy, S. Mukherjee, V. Kleiner, E. Koren, and E. Hasman, Valley-addressable monolayer lasing through spin-controlled Berry phase photonic cavities, Science **381**, 1429 (2023).
[20] R. Jia, S. Kumar, T. C. Tan, A. Kumar, Y. J. Tan, M. Gupta, P. Szriftgiser, A. Alphones, G. Ducournau, and R. Singh, Valley-conserved topological integrated antenna for 100-Gbps THz 6G wireless, Sci. Adv. **9**, 1 (2023).
[21] M. I. Shalaev, W. Walasik, A. Tsukernik, Y. Xu, and N. M. Litchinitser, Robust topologically protected transport in photonic crystals at telecommunication wavelengths, Nat. Nanotechnol. **14**, 31 (2019).
[22] J. W. You, Q. Ma, Z. Lan, Q. Xiao, N. C. Panoiu, and T. J. Cui, Reprogrammable plasmonic topological insulators with ultrafast control, Nat. Commun. **12**, 1 (2021).
[23] Y. Kawaguchi, D. Smirnova, F. Komissarenko, S. Kiriushechkina, A. Vakulenko, M. Li, A. Alù, and A. B. Khanikaev, Pseudo-spin switches and Aharonov-Bohm effect for topological boundary modes, Sci. Adv. **10** (2024).
[24] W. Wang, Y. J. Tan, T. C. Tan, A. Kumar, P. Pitchappa, P. Szriftgiser, G. Ducournau, and R. Singh, On-chip topological beamformer for multi-link terahertz 6G to XG wireless, Nature (London) **632**, 522 (2024).
[25] See Supplemental Material at http://link.aps.org/supplemental/10.1103/PhysRevLett.134.203803, which includes Refs. [26,27], for details on the valley topological state, frameworks for valley-robust transport, Berry curvature distribution, sample fabrication and measurement, chirality source setup, edge band evolution, experimental and simulated results of one-way valley-robust transport, photonic application, and material properties.
[26] D. M. Pozar, *Microwave Engineering*, Fourth Editions (John Wiley & Sons, Inc., New York, 2012).
[27] A. G. Gurevich and G. A. Melkov, *Magnetization Oscillations and Waves* (CRC Press, Boca Raton, New York, London, and Tokyo 1996).
[28] C. A. Rosiek, G. Arregui, A. Vladimirova, M. Albrechtsen, B. Vosoughi Lahijani, R. E. Christiansen, and S. Stobbe, Observation of strong backscattering in valley-Hall photonic topological interface modes, Nat. Photonics **17**, 386 (2023).

[29] D. Yu, S. Arora, and L. Kuipers, Impact of transforming interface geometry on edge states in valley photonic crystals, Phys. Rev. Lett. **132**, 116901 (2024).
[30] A. Kumar, Y. J. Tan, N. Navaratna, M. Gupta, P. Pitchappa, and R. Singh, Slow light topological photonics with counter-propagating waves and its active control on a chip, Nat. Commun. **15**, 926 (2024).
[31] X. Xi, I. Chernobrovkin, J. Kǒ, and M. B. Kristensen, A soft-clamped topological waveguide for phonons, arXiv: 2408.08717v1.
[32] F. D. M. Haldane and S. Raghu, Possible realization of directional optical waveguides in photonic crystals with broken time-reversal symmetry, Phys. Rev. Lett. **100**, 013904 (2008).
[33] S. Raghu and F. D. M. Haldane, Analogs of quantum-Hall-effect edge states in photonic crystals, Phys. Rev. A **78**, 033834 (2008).
[34] Z. Wang, Y. D. Chong, J. D. Joannopoulos, and M. Soljačić, Reflection-free one-way edge modes in a gyromagnetic photonic crystal, Phys. Rev. Lett. **100**, 013905 (2008).
[35] Z. Wang, Y. Chong, J. D. Joannopoulos, and M. Soljačić, Observation of unidirectional backscattering-immune topological electromagnetic states, Nature (London) **461**, 772 (2009).
[36] Y. Poo, R. X. Wu, Z. Lin, Y. Yang, and C. T. Chan, Experimental realization of self-guiding unidirectional electromagnetic edge states, Phys. Rev. Lett. **106**, 093903 (2011).
[37] G. G. Liu *et al.*, Topological Anderson insulator in disordered photonic crystals, Phys. Rev. Lett. **125**, 133603 (2020).
[38] G.-G. Liu, P. Zhou, Y. Yang, H. Xue, X. Ren, X. Lin, H. Sun, L. Bi, Y. Chong, and B. Zhang, Observation of an unpaired photonic Dirac point, Nat. Commun. **11**, 1873 (2020).
[39] Y. Wang *et al.*, Hybrid topological photonic crystals, Nat. Commun. **14**, 4457 (2023).
[40] J.-C. Lu, X.-D. Chen, W.-M. Deng, M. Chen, and J.-W. Dong, One-way propagation of bulk states and robust edge states in photonic crystals with broken inversion and time-reversal symmetries, J. Opt. **20**, 075103 (2018).
[41] S. Stützer, Y. Plotnik, Y. Lumer, P. Titum, N. H. Lindner, M. Segev, M. C. Rechtsman, and A. Szameit, Photonic topological Anderson insulators, Nature (London) **560**, 461 (2018).
[42] X. Ni, D. Purtseladze, D. A. Smirnova, A. Slobozhanyuk, A. Alù, and A. B. Khanikaev, Spin- and valley-polarized one-way Klein tunneling in photonic topological insulators, Sci. Adv. **4**, 1 (2018).
[43] W. Yao, S. A. Yang, and Q. Niu, Edge states in graphene: From gapped flat-band to gapless chiral modes, Phys. Rev. Lett. **102**, 096801 (2009).
[44] R. Xi, Q. Chen, Q. Yan, L. Zhang, F. Chen, Y. Li, H. Chen, and Y. Yang, Topological chiral edge states in deep-subwavelength valley photonic metamaterials, Laser Photonics Rev. **2200194**, 1 (2022).
[45] X. D. Chen, F. L. Shi, H. Liu, J. C. Lu, W. M. Deng, J. Y. Dai, Q. Cheng, and J. W. Dong, Tunable electromagnetic flow control in valley photonic crystal waveguides, Phys. Rev. Appl. **10**, 044002 (2018).
[46] X. Xi, J. Ma, S. Wan, C. H. Dong, and X. Sun, Observation of chiral edge states in gapped nanomechanical graphene, Sci. Adv. **7**, 1 (2021).
[47] Y. Feng, Z. Zhang, F. Qin, Z. Lan, W. E. I. Sha, and Y. Xu, Bound valley edge states in the continuum, Opt. Lett. **47**, 3107 (2022).
[48] Y. C. Zhou, H. S. Lai, J. L. Xie, X. C. Sun, C. He, and Y. F. Chen, Magnetic corner states in a two-dimensional gyromagnetic photonic crystal, Phys. Rev. B **107**, 014105 (2023).
[49] X.-D. Chen, F.-L. Zhao, M. Chen, and J.-W. Dong, Valley-contrasting physics in all-dielectric photonic crystals: Orbital angular momentum and topological propagation, Phys. Rev. B **96**, 020202(R) (2017).
[50] P. Zhou, G. G. Liu, Y. Yang, Y. H. Hu, S. Ma, H. Xue, Q. Wang, L. Deng, and B. Zhang, Observation of photonic antichiral edge states, Phys. Rev. Lett. **125**, 263603 (2020).
[51] M. Liu, S. Xia, W. Wan, J. Qin, H. Li, C. Zhao, L. Bi, and C. Qiu, Broadband mid-infrared non-reciprocal absorption using magnetized gradient epsilon-near-zero thin films, Nat. Mater. **22**, 1196 (2023).
[52] N. Morali, R. Batabyal, P. K. Nag, E. Liu, Q. Xu, Y. Sun, B. Yan, C. Felser, N. Avraham, and H. Beidenkopf, Fermi-arc diversity on surface terminations of the magnetic Weyl semimetal $Co_3Sn_2S_2$, Science **365**, 1286 (2019).
[53] F. Dirnberger *et al.*, Magneto-optics in a van Der Waals magnet tuned by self-hybridized polaritons, Nature (London) **620**, 533 (2023).
[54] H. Xue *et al.*, Three-dimensional valley-contrasting sound, Sci. Adv. **10**, 1 (2024).
[55] M. C. Rechtsman, J. M. Zeuner, Y. Plotnik, Y. Lumer, D. Podolsky, F. Dreisow, S. Nolte, M. Segev, and A. Szameit, Photonic floquet topological insulators, Nature (London) **496**, 196 (2013).
[56] Y. Ding, Y. Peng, Y. Zhu, X. Fan, J. Yang, B. Liang, X. Zhu, X. Wan, and J. Cheng, Experimental demonstration of acoustic Chern insulators, Phys. Rev. Lett. **122**, 014302 (2019).
[57] J. Deng *et al.*, Observing the quantum topology of light, Science **378**, 966 (2022).
[58] S. Klembt *et al.*, Exciton-polariton topological insulator, Nature (London) **562**, 552 (2018).
[59] Z. Zhang, P. Delplace, and R. Fleury, Superior robustness of anomalous non-reciprocal topological edge states, Nature (London) **598**, 293 (2021).
[60] E. Lustig, S. Weimann, Y. Plotnik, Y. Lumer, M. A. Bandres, A. Szameit, and M. Segev, Photonic topological insulator in synthetic dimensions, Nature (London) **567**, 356 (2019).
[61] J. Chen, Y. Zheng, S. Yang, F. Shi, Z.-Y. Li, and C.-W. Qiu, One-way valley-robust transport in edge-tailored photonic crystals, Figshare, Dataset, 10.6084/m9.figshare.28879328.v2 (2025).